Formation of Fine Microstructure in Weld Metal Containing Mn-Ti based Oxides

Hidenori NAKO*1, Yoshitomi OKAZAKI*1, Dr. Hitoshi HATANO*1, Ken YAMASHITA*2, Hideaki TAKAUCHI*2

*1 Materials Research Laboratory, Technical Development Group
*2 Welding Process Dept., Technical Center, Welding Business

The formation of fine acicular ferrite microstructure and toughness improvement have been observed in a welding metal in which inclusion particles containing Mn-Ti based oxide are dispersed. The inclusion particles are composed of $MnTi_2O_4$, TiO_2, amorphous and MnS phases, while the acicular ferrite has been nucleated from the $MnTi_2O_4$ phase. The Baker-Nutting crystal orientation relationship has been found between $MnTi_2O_4$ phase and acicular ferrite, whereas the Kurdjumov-Sachs orientation relationship has been found between the prior austenite phase and acicular ferrite. It has been discovered that the favorable lattice matching at the interface between the prior austenite phase and acicular ferrite may possibly have promoted the nucleation and growth of acicular ferrite, as well as the lattice matching at the $MnTi_2O_4$/ acicular ferrite interface.

Introduction

As steel structures such as ships, buildings, and offshore structures become larger and are used in environments at lower temperatures, higher strength and toughness are required for weld metals. In the strengthening mechanism of steel, grain boundary strengthening (grain refinement strengthening) is known to improve strength and toughness simultaneously.[1] Hence, realizing a weld metal that combines high strength and high toughness requires technology to refine the microstructure of weld metal.

Acicular ferrite (hereinafter referred to as "AF") is a microstructure that is generated from inclusion particles, as nucleation sites, in the weld metal of low carbon/low-alloy steel and in the heat-affected zones of welds. This microstructure provides high toughness.[2)-4)] The inclusions that are known to act as the nucleation sites for AF generation are oxides,[5)] nitrides,[4)] and sulfides.[6)] In particular, Ti oxides such as TiO,[7)-9)] Ti_2O_3,[9)] and TiO_2[10)] effectively promote the formation of AF.

The following three theories have been proposed for the generation mechanism of AF from inclusions as a nucleation site.

(1) The decrease in inclusion/AF interface energy: When an interface with favorable lattice matching is formed between an inclusion and AF, the interface energy between the inclusion and AF decreases, facilitating the nucleation of AF on the surface of the inclusion. This is a concept focusing on the structural energy component of the interface energy and has been studied for a long time.[8), 11)] In recent years, researches based on chemical energy have also been conducted.[12)]

(2) A compositional change of austenite phase around inclusions: This is the theory that the composition of the austenite phase around inclusions changes before the AF is generated such that the driving force for AF generation increases. The Mn-depleted zone is cited as an example.[13)] It has been shown that, when Mn, an austenite stabilizing element, is absorbed by inclusions, a Mn-depleted zone is formed in the vicinity of the inclusions, raising the Ae_3 temperature. Furthermore, Gregg has pointed out the existence of a C-depleted zone in which C is another austenite stabilizing element.[10)]

(3) The introduction of strain and dislocations to the austenite phase around inclusions: This is the theory that the difference in the coefficient of thermal expansion between inclusions and austenite phase causes strain and dislocations in austenite phase around inclusions, promoting the generation of AF; however, there is little experimental evidence. It has been shown by calculation that the contribution of strain energy to the driving force of ferrite transformation is small.[14)] On the other hand, Sumino describes the possibility that the dislocations around inclusions act as the preferred nucleation sites for AF.[15)]

Dowling et al. have reported that inclusions contribute to the generation of AF as mere heterogeneous nuclei and the influence of inclusion species is small.[16)]

As described, many studies have been conducted on the inclusions that generate AF and on the mechanism of how these inclusions generate AF; however, most studies have been made on single phase inclusions consisting of simple, pure oxides. On the other hand, a weld metal contains a plurality of deoxidizing elements and highly enriched oxygen; hence, more complex inclusion particles are considered to be formed. In the case of such complex inclusions, the mechanism of AF generation and their relationships with mechanical properties have not sufficiently been clarified. Against this backdrop, Kobe Steel studied the complex inclusion

particles containing Mn-Ti based oxides, including their influence on the AF structure and mechanical properties, and also studied the mechanism of AF generation. An outline follows:

1. Experimental method

1.1 Weld metals

Two types of weld metals were prepared as testing materials: i.e., a Ti-free material containing low Mn and no Ti, and Ti-added material with high Mn. For welding, low carbon steel plates were prepared, each having a thickness of 25 mm and a 10°V groove. Submerged arc welding (hereinafter referred to as "SAW") was performed under the conditions of root opening, 15 mm; welding current, 425 A; voltage, 30 V; welding speed, 5.8 mm/s; and inter-pass temperature, 180 ℃ to 200 ℃. **Table 1** shows the compositions of the weld metals. The contents of P, S, and N were lower than 0.008, 0.003 and 0.010 mass%, respectively. Some of the weld metal thus obtained was subjected to post weld heat treatment (PWHT) at 640 ℃ for 108 ks.

1.2 Microstructure observations

Weld metal consists of an as-welded zone, which has an as-solidified matrix structure, and a reheated zone with a matrix structure that has been changed due to the thermal influence of subsequent welding passes. The grain size of the prior austenite in a reheated zone is smaller than that in an as-welded zone and changes with the distance from the melted part of the subsequent pass. When prior austenite grains are rather small, the amount of AF generation is affected by the size of prior austenite grains.[17), 18)] For this reason, when comparing the AF structures in the reheated zones, the difference in the grain size of the prior austenite due to different observation points must be taken into account, which is cumbersome. Hence, in the present study, microstructure observations were conducted in the as-welded zones contained in the weld metal formed during the final pass, since these zones have sufficiently large prior austenite grains. The surfaces that are vertical to the welding direction were mirror-polished for observation under an optical microscope. Photographs were taken in two fields at 1000x magnification. The number density and the average circle-equivalent diameter of the inclusions in the photos were determined by image analysis. Due to photographic resolution, inclusions of 0.5μm or larger, in terms of circle-equivalent diameter, were analyzed. Subsequently, the same samples were etched with 3% Nital solution and the microstructures of their matrixes were observed under the optical microscope. In addition, inclusion particles and the AF structures nucleated from these were selected, and the surface etched layers were polished off. A scanning electron microscope, JEOL JSM-6500F, was used to analyze the electron backscatter diffraction (EBSD) patterns to determine the crystal orientation of AF. A step size of 0.1μm was selected for the EBSD measurement in consideration of the ferrite phase and austenite phase. Furthermore, transmission electron microscopy (TEM) observations were carried out using JEOL JEM-2010F to identify the phase constituting the inclusion particles that became the nucleation site for AF generation. From the observation fields that had been subjected to EBSD measurement above, the regions containing inclusion particles were picked up by the focused ion-beam system (FB2000A) and were processed into thin film samples for the TEM observation. The TEM observations were carried out at an accelerating voltage of 200 kV. In order to identify the inclusion phase, the elements constituting the inclusions were determined by the energy dispersive X-ray spectroscopy (EDS). The crystal structure was determined by the selected area diffraction pattern. In addition, Kikuchi's pattern analysis[19)] was applied to analyze the crystal orientation relationship between the inclusion phase and AF.

1.3 Mechanical properties

The yield strength (YS) and tensile strength (TS) were examined for the weld metals in an as-welded state, which is the state not subjected to post-welding heat treatment, etc., and for the weld metals after being processed by PWHT. Each tensile test piece (JIS Z 3111, A2 type) was collected from the center of the corresponding weld metal in a direction parallel to the welding direction. In order to evaluate the impact toughness, V-notch Charpy test pieces (3 pieces), in accordance with JIS Z 3111,

Table 1 Chemical compositions of weld metals (mass%)

	C	Si	Mn	Al	Ni	Cr	Mo	Ti	O	Fe
Ti free	0.06	0.07	1.20	0.005	1.54	0.28	0.78	0.001	0.047	bal.
Ti added	0.13	0.13	1.65	0.005	1.60	0.28	0.77	0.051	0.025	bal.

were collected from the central part of each weld metal and in the welding direction so that each notch was positioned at the joining portion of the respective welding pass. Charpy impact absorbed energy, $vE_{-30℃}$, was evaluated by the average value of the results for three test pieces at -30 ℃.

2. Experimental results and discussions

2.1 Microstructure and mechanical properties

Fig. 1 shows the optical micrographs of the weld metals. In the Ti-free material, a coarse bainite microstructure is observed across the field, in which the bainite microstructure has substructures, such as packets and blocks, generated from the prior austenite grain boundaries. On the other hand, Ti-added material exhibits an extremely fine microstructure. It has been observed that some of the crystal grains that constitute this fine microstructure have been generated radially from inclusion particles, as indicated by the arrow in Fig. 1(d). These are the AFs generated from inclusion particles as their nucleation sites. The fine crystal grain, which seems to exist irrespective of the inclusion particles at first glance, is presumed to be AF formed on the inclusion particle inside the weld metal, or has undergone sympathetic nucleation from the AF that was generated earlier.[20]

Fig. 2 shows the size distributions of inclusion particles in the weld metals of Ti-free material and Ti-added material. In the Ti-free material, which contains a greater amount of oxygen, there is observed a trend for the relatively fine inclusion particles with a circle-equivalent diameter of 1.00μm or less to increase in number. On the other hand, no significant difference due to the presence or absence of Ti addition has been detected in the number density of the coarse inclusion particles exceeding the circle-equivalent diameter of 1.00μm. The mean circle-equivalent diameters of inclusion particles were 0.80μm for Ti-free material and 0.83μm for Ti-added material, showing that the values are almost the same.

Table 2 shows the mechanical properties of the weld metals. In the as-welded state, the Ti-added

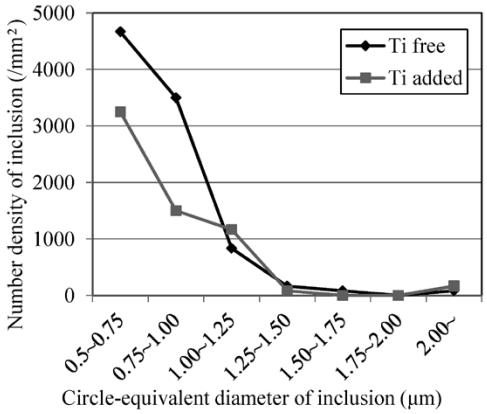

Fig. 2 Size histogram of inclusion particles in the weld metals

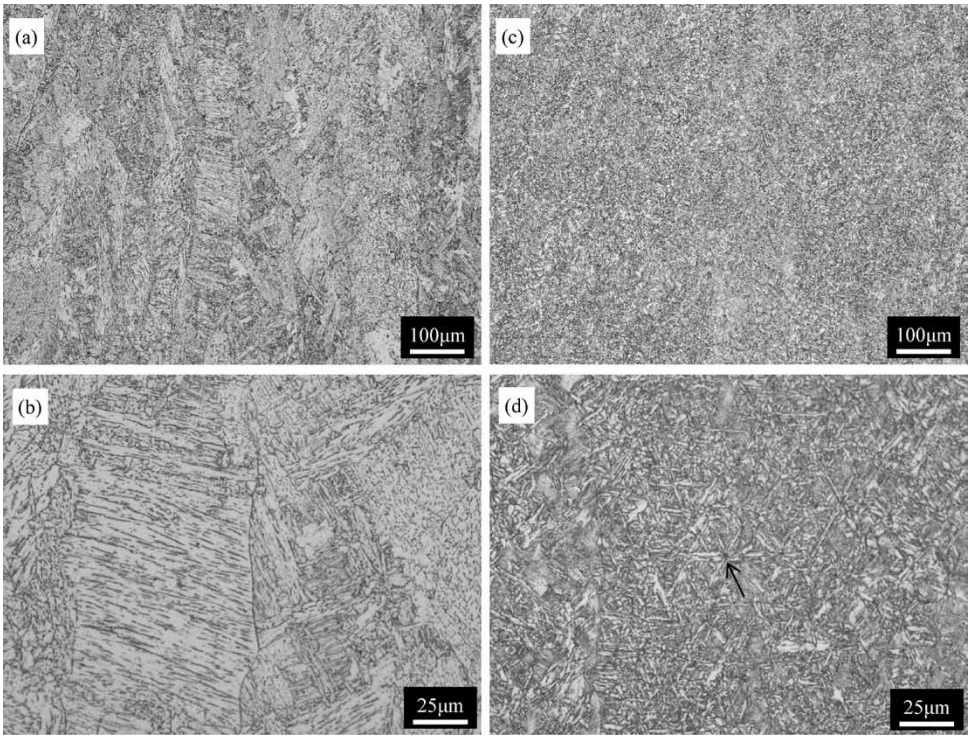

Fig. 1 Optical micrographs of the (a, b) Ti free and (c, d) Ti-added weld metals

Table 2 Mechanical properties of weld metals

	As weld			After PWHT		
	YS (MPa)	TS (MPa)	vE-30°C (J)	YS (MPa)	TS (MPa)	vE-30°C (J)
Ti free	580	672	53	454	575	59
Ti added	773	927	72	701	776	60

material exhibits a yield strength approximately 200 MPa higher than, and a toughness value that is substantially equal to, those of the Ti-free material. This is considered to be attributable to the microstructure refinement by the AF generated in the Ti-added material. The Ti-added material also exhibits a favorable balance of strength and toughness after the PWHT.

2.2 Mechanism of AF generation in Ti-added material

2.2.1 Inclusion phase acting as the nucleation site for AF generation

In the Ti-added material, it is worthy of note that AF has been generated from inclusions as its nucleation site. Prior austenite grain size has been reported to influence the generation of AF structure.[17), 18)] The present weld metals have been prepared under identical welding conditions and have almost the same prior austenite grain sizes. Hence, their influence on AF generation is presumed to be negligible. The number of inclusions that act as the nucleation sites for AF generation is considered to be the product of the total number of inclusions and AF generation frequency in the individual inclusion particle; however, as shown in Fig. 2, the number of inclusion particles in the Ti-added material is smaller than that of the Ti-free material. Therefore, the inclusion particles in the Ti-added material are presumed to contain a phase that is more likely to generate AF, i.e., has a higher AF generation potential.

Fig. 3 shows an inverse pole figure (IPF) map of the field encompassing the inclusion indicated by an arrow in Fig. 1 (d) and the peripheral AF structure.[21)] The black part (unanalyzable point) near the center is an inclusion particle providing the nucleation site for the generation of AF crystal grains (indicated as "AF1", "AF2" in the figure). Also observed are several crystal grains that are not in contact with the inclusion particle, but extending radially from it. These are considered to be AF generated from inclusion particles outside the observation surface, or crystal grains that have undergone sympathetic nucleation from the AF.[20)] There also are almost equiaxial crystal grains in contact with the inclusion particle. It is not clear whether these grains have

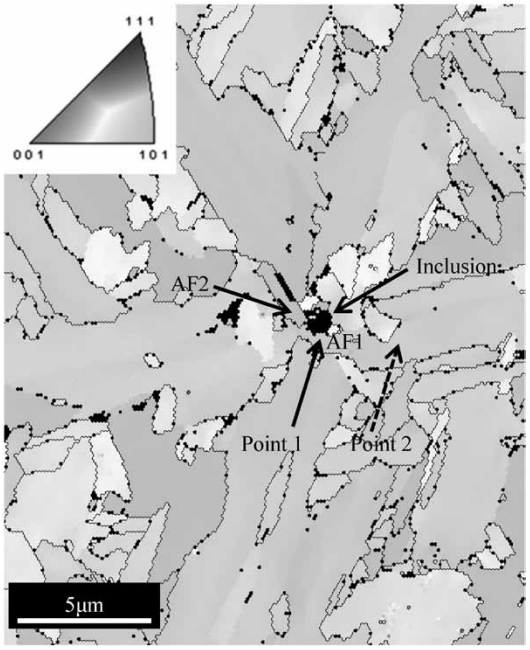

Fig. 3 Inverse pole figure map of the Ti added weld metal [21)]

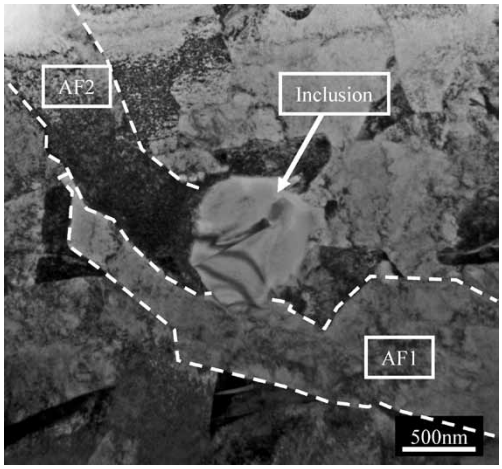

Fig. 4 Bright field image of the Ti added weld metal [21)]

been nucleated on the surfaces of other inclusion particles, or have grown from other nucleation sites and have touched the inclusion particle incidentally. Therefore, only two AF particles, AF1 and AF2, are confirmed to have been generated from the inclusion particle in Fig. 3.

Fig. 4 is the TEM bright-field image of the area including the inclusion particle in Fig. 3 and its surrounding matrix.[21)] Once again, this confirms that the AF1 and AF2 observed in Fig. 3 have been generated from the inclusion particle as their nucleation sites. **Fig. 5** is an EDS mapping of the inclusion particle.[21)] The inclusion particle comprises four parts: namely (1) the part where both Ti and Mn are enriched, occupying a large area from the center to the lower left of the inclusion particle; (2) the part where both Si and Mn are enriched, surrounding the Ti and Mn enriched part; (3) the

part where Ti is enriched, as observed in the upper left of the inclusion particle; and (4) the part where Mn is enriched, as observed in the upper right and the far right of the inclusion particle. The selected area diffraction patterns (**Fig. 6**) have identified the fact that the part enriched by Ti/Mn, the part enriched by Si/Mn and the part enriched by Ti are $MnTi_2O_4$, amorphous phase, and TiO_2, respectively. In addition, a separately conducted EDS point analysis has detected S, indicating that the Mn-enriched part is MnS.

Comparison of these phases, constituting the inclusion particle, with the locations of AF1 and AF2 has revealed that AF1 is in contact only with the $MnTi_2O_4$ phase, and AF2 is in contact with the $MnTi_2O_4$ phase, TiO_2 phase, and amorphous phase. Also, it has been found that both AF1 and AF2 have been generated at positions away from MnS. There seem to be few reports indicating that, among the three phases in contact with AF2, the amorphous

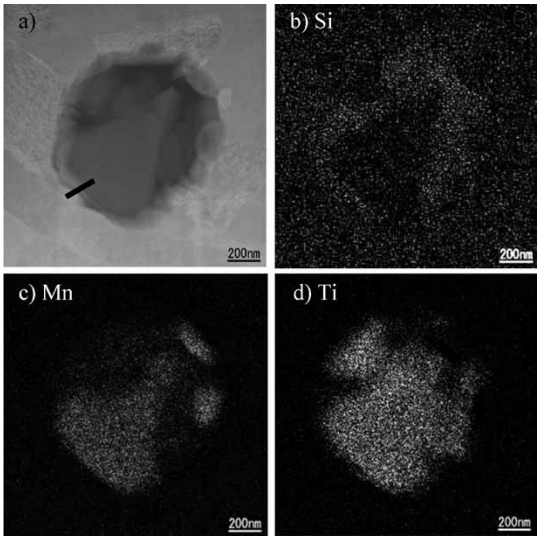

Fig. 5 (a) TEM image, (b)～(d) EDS mappings of Si, Mn and Ti of the inclusion particle observed in Fig. 4[21]

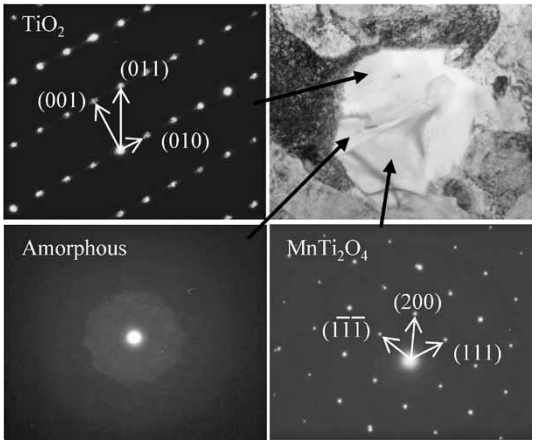

Fig. 6 Selected area diffraction patterns of the inclusion particle observed in Fig. 4[21]

phase promotes AF generation. It has been reported that both the $MnTi_2O_4$ phase and TiO_2 phase function as the nucleation site of AF generation.[22), 23), 10)] The fact that AF1 is in contact only with the $MnTi_2O_4$ phase suggests that the $MnTi_2O_4$ phase acts most effectively as the nucleation site for AF generation.

2.2.2 AF generation mechanism via $MnTi_2O_4$

The generation mechanism of AF1, which is deemed to have been nucleated on $MnTi_2O_4$ phase, has been studied from the viewpoints of the compositional change of the peripheral matrix and the lattice matching with AF.

Fig. 7 shows the results of measurements on the Mn and Ti concentrations along the bold line from $MnTi_2O_4$ to AF1 in Fig. 5(a). No Mn-depleted zone has been detected clearly, due to the unevenness of the data, on the side of AF1 and in the vicinity of the $MnTi_2O_4$/AF1 interface, although the Mn concentration seems to have been decreased slightly. The formation of the Mn-depleted zone is a result of Mn diffusing from the austenite phase into the inclusions. In the case of the weld metals of the present study, it is considered that the cooling after welding has been too rapid to secure enough time for the diffusion of Mn. According to Shigesato et al.,[13)] a zone in which Mn has been depleted by 0.4mass% has been detected in a sample with AF structure occupying at least 80% an area fraction. In the present study, however, the microstructure of the Ti-added material exhibits AF almost across the field, which makes it difficult to explain the AF generation on the basis of the Mn-depleted zone in the Ti-added material. Furthermore, almost no Ti, a ferrite stabilizing element, was detected in AF1.

Fig. 8 is an [101] pole figure of $MnTi_2O_4$, in (100) of AF1 and $MnTi_2O_4$. The figure has been obtained by analyzing their crystal orientations.[21)] The $\{001\}_{MnTi_2O_4}$ and $\{001\}_{AF1}$, as well as $<110>_{MnTi_2O_4}$ and

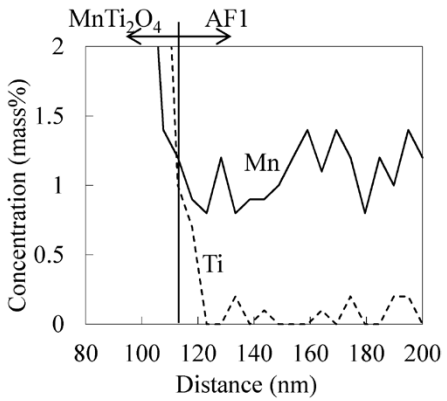

Fig. 7 Mn and Ti concentration profiles along the bold line in Fig. 5(a)

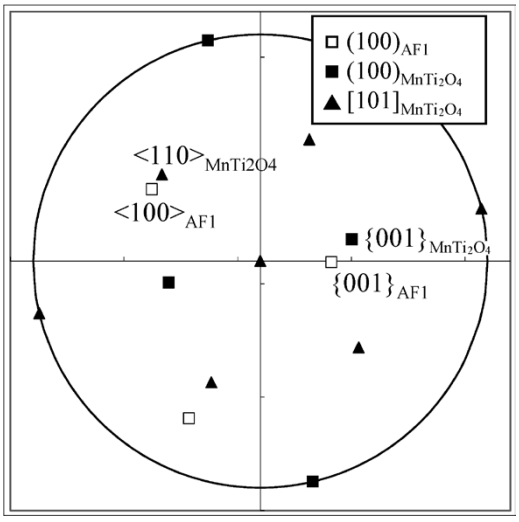

Fig. 8 Stereographic projection of the AF1 and the $MnTi_2O_4$ shown in Fig. 4[21)]

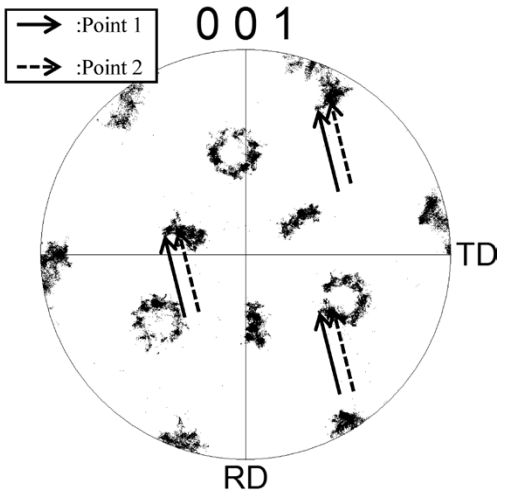

Fig. 9 (001) pole figure of the area corresponding to Fig. 3[21)]

$<100>_{AF1}$, are close to each other. This result suggests that the following crystal orientation relationship of Baker-Nutting (B-N relationship) holds in $MnTi_2O_4$ and AF1.

$(001)_{MnTi_2O_4}//(001)_{AF}$, $[110]_{MnTi_2O_4}//[100]_{AF}$

It should be noted, however, that the probability that B-N relationship occurs by chance, the probability assuming the allowable misorientation of 15° [24)] and determined by the technique of Grong et al.[11)], is relatively high at 10%; thus, it is possible that the B-N relationship has been established only by chance. Against this backdrop, the crystal orientation of AF1 has been analyzed in more detail. The (001) pole figure of the measurement area in Fig. 3 is shown in **Fig. 9**.[21)] This measurement area is located inside one crystal grain of prior austenite, resulting in a highly symmetric pole figure roughly in accordance with the Kurdjumov-Sachs crystal orientation relationship (K-S relationship).[25)] It is noteworthy that the crystal orientation (Point 1) of AF 1 in the vicinity of the inclusion particle is displaced by 5.5° from the ideal K-S relationship. On the other hand, a crystal orientation close to a K-S relationship has been detected at Point 2, which is away from the inclusion particle in AF1. These results indicate that the AF1 nucleates with a crystal orientation slightly deviating from the K-S relationship, and has changed its crystal orientation such that it approaches the K-S relationship in the process of its growth. This is the same trend as reported by Takada et al. on the AF nucleated from TiO,[26)] and is considered attributable to AF1 nucleating preferentially in accordance with the B-N relationship. Bramfit has reported that the carbonitride, which has a planar disregistry below 12%, functions as the nucleus for the solidification of BCC iron because of their favorable lattice matching.[27)] When the fact that $MnTi_2O_4$ has a cubic crystal structure with a lattice constant of 0.862 8 nm,[28)] the planar disregistry[27)] at the establishment of the B-N relationship is sufficiently low at 6.67%. From this, the fact that $MnTi_2O_4$, having an interface where the B-N relationship holds, is considered to have realized a favorable lattice matching with AF, facilitating the nucleation of AF.

Furthermore, it is presumed that AF retaining the K-S relationship with austenite phase has low interface energy with the austenite phase,[29)] further promoting the nucleation and growth. In the AF immediately after its nucleation, a crystal orientation close to the K-S relationship has been detected in addition to the B-N relationship. This suggests the possibility that a crystal orientation that is close to the K-S relationship may have been selected during the nucleation while satisfying the B-N relationship. The nucleation barrier energy ΔG^* when AF nucleates on inclusion is expressed by the following equations in the classical nucleation theory.

$$\Delta G^* = \frac{16\pi\sigma^3_{AF/\gamma}}{3(\Delta G_V + \Delta G_S)^2} \cdot f(\theta) \quad \cdots\cdots (1)$$

$$f(\theta) = \frac{(2+\cos\theta)(1-\cos\theta)^2}{4} \quad \cdots\cdots (2)$$

$$\cos\theta = \frac{\sigma_{\gamma/X} - \sigma_{AF/X}}{\sigma_{AF/\gamma}} \quad \cdots\cdots (3)$$

where

$\sigma_{AF/\gamma}$: AF/austenite phase interface energy
$\sigma_{\gamma/X}$: austenite phase/inclusion interface energy
$\sigma_{AF/X}$: AF/inclusion interface energy
ΔG_V : nucleation driving force, and
ΔG_S : strain energy.

When the B-N relationship and K-S relationship are established simultaneously, the values of $\sigma_{AF/X}$ and $\sigma_{AF/\gamma}$ decrease. Therefore, it is considered that ΔG^* decreases as compared with the case where K-S and B-N relationships are established

independently,[21] facilitating the nucleation of AF.

The reason considered for the change in the crystal orientation of AF, the change that takes place as it approaches the K-S relationship during the growth process, is that this lowers the energy of the AF/austenite interface. In other words, although AF selects a crystal orientation that can predominate over both the interface energies of $MnTi_2O_4$ and austenite phase at the time of its nucleation, it changes its crystal orientation so that the energy of the interface becomes lower as the interface with the austenite phase increases during its growth process. From the above, it is concluded that the interface energy between AF and nucleation-site inclusions strongly affects the nucleation and growth of AF, and so does the interface energy between the austenite phase and AF.

It should be noted that both the B-N relationship between the AF and $MnTi_2O_4$ phase and the K-S relationship between the AF and prior austenite phase have been detected simultaneously at the time of nucleation. This suggests the possibility that, prior to AF generation, a specific crystal orientation relationship (herein referred to as the X-A relationship) has existed between the $MnTi_2O_4$ phase and prior austenite phase. In general, inclusions in weld metal are formed in molten iron, and the resulting crystal orientation relationship with prior austenite phase is considered to be random.[30] This consideration leads to the interpretation that, among the $MnTi_2O_4$ particles with various crystal orientations, only the $MnTi_2O_4$ particles that satisfy the X-A relationship by chance have allowed the simultaneous establishment of B-N and K-S relationships, preferentially acting as the nucleation sites for AF. On the other hand, the above concept is based on the assumption that the inclusions generated in molten iron are solid inclusions, and if the solidification temperature of the inclusions is low, there is a possibility that a specific /non-random crystal orientation relationship may be established with the austenite phase. That is, when inclusions having existed in a liquid state at high temperature solidify in the austenite temperature region, there may be cases where the crystallization occurs with a crystal orientation relationship having a favorable lattice matching with the peripheral austenite phase. Kobe Steel's analysis[21] has revealed that a specific orientation relationship can exist between the austenite phase and $MnTi_2O_4$ phase. This orientation relationship achieves a relatively favorable planer disregistry of 8.6% against the austenite phase while allowing the simultaneous establishment of K-S and B-N relationships with a deviation of 5.3° from the ideal direction in the subsequent AF nucleation. There are many simple oxides having high solidification temperatures; however, Blais et al. have pointed out on the basis of their thermodynamic calculation that the solidification point of $MnTi_2O_4$ can be lower than that of steel.[22] The relationships among the solidification point of inclusions and the crystal orientations of the AF, inclusions and austenite phase, as well as the relationship with the AF generation, will be the subjects of future study.

Conclusions

The generation behavior and mechanical properties of AF structures have been studied using weld metals with the dispersion of composite inclusion particles including Mn-Ti based oxide, and the following results were obtained:

- Of the plurality of phases constituting the inclusion particles, $MnTi_2O_4$ phase predominantly functions as the nucleation site for AF generation.
- From the viewpoint of nucleation and growth, the interface energy between $MnTi_2O_4$ phase/ austenite phase and AF has a dominant influence on AF generation.
- Weld metals with the AF structure exhibit a favorable balance of strength and toughness.

References

1) M. Maki. Tekko no soshiki seigyo --Sono genri to hoho (Microstructure control of steel--Its principle and method). 1st Edition, Uchida Rokakuho Publishing Co. Ltd., 2015, pp. 125-127.
2) I. Watanabe et al. Journal of the Japan Welding Society (Journal of JWS). 1980, Vol. 49, No. 11, pp. 772-780.
3) N. Mori et al. Journal of the Japan Welding Society (Journal of JWS). 1981, Vol. 50, No. 8, pp. 786-793.
4) K. Yamamoto et al. ISIJ Int. 1996, Vol. 36, No. 1, pp. 80-86.
5) Y. Horii et al. Q. J. Jpn. Weld. Soc. 1995, Vol. 13, No. 4, pp. 500-507.
6) T. Hanamura et al. ISIJ Int. 1999, Vol. 39, No. 11, pp. 1188-1193.
7) T. Yamada et al. ISIJ Int. 2009, Vol. 49, No. 7, pp. 1059-1062.
8) A. R. Mills et al. Mater. Sci. Tech. 1987, Vol. 3, pp. 1051-1061.
9) J. M. Gregg et al. Acta Metall. Mater. 1994, Vol. 42, No. 10, pp. 3321-3330.
10) J. M. Gregg et al. Acta Mater. 1997, Vol. 45, No. 2, pp. 739-748.
11) O. Grong et al. Metall. Mater. Trans. A. 1995, Vol. 26A, No. 3, pp. 525-534.
12) K. Kasai et al. TETSU-TO-HAGANE. 2010, Vol. 96, No. 3, pp. 123-128.
13) G. Shigesato et al. TETSU-TO-HAGANE. 2001, Vol. 87, No. 2, pp. 93-100.
14) T. Minote et al. Iron and Steel Institute of Japan, 1995, pp. 65-74.
15) K. Sumino. Iron and Steel Institute of Japan, 1998, pp. 17-43.
16) J. M. Dowling et al. Metall. Trans. A. 1986, Vol. 17A, No. 9,

pp. 1611-1623.
17) D. Zhang et al. Acta Mater. 2010, Vol. 58, pp. 1369-1378.
18) F. J. Barbaro et al. Mater. Sci. Tech. 1989, Vol. 5, No. 11, pp. 1057-1068.
19) S. Zaefferer. J. Appl. Cryst. 2000, Vol. 33, pp. 10-25.
20) K. M. Wu et al. Mater. Charact. 2004, Vol. 52, pp. 121-127.
21) H. Nako et al. ISIJ Int. 2014, Vol. 54, No. 7, pp. 1690-1696.
22) C. Blais et al. Sci. Technol. Weld. Join. 1999, Vol. 4, No. 3, pp. 143-150.
23) Y. Okazaki et al. Quarterly Journal of the Japan Welding Society. 2009, Vol. 27, No. 2, pp. 131-138.
24) C. Lee et al. ISIJ Int. 2011, Vol. 51, No. 12, pp. 2036-2041.
25) S. Morito et al. Acta Mater. 2003, Vol. 51, pp. 1789-1799.
26) A. Takada et al. Quarterly Journal of the Japan Welding Society. 2013, Vol. 31, No. 1, p. 33-40.
27) B. L. Bramfitt. Metall. Trans. 1970, Vol. 1, No. 7, pp. 1987-1995.
28) Y. Huang et al. J. Magnetism and Magnetic Mater. 2012, Vol. 324, pp. 2075-2081.
29) T. Nagao et al. Metall. Mater. Trans. A. 2006, Vol. 37A, No. 3, pp. 929-937.
30) H. K. D. H. Bhadeshia et al. Mathematical Modeling of Weld Phenomena. The Institute of Materials, 1993, pp. 109-180.